論文 84-21-5-13

A Thermal Model for Silicon-on-Insulator Multilayer Structure in Silicon Recrystallization Using Tungsten Lamp

(텅스텐 램프를 이용한 실리콘 재결정시의 SOI 다층구조에 대한 열적모델)

慶 宗 旻*

(Chong Min Kyung)

要 約

양면에서 텅스텐 램프를 조사하는 실리콘 재결정시의 SOI(silicon-on-insulator) 다층구조에 대한 1차원적 온도 및 열원(熱源)의 분포를 SOR(successive over- relaxation)방법을 이용하여 정상상태의 열방정식의 해로부터 구하였다. 열원의 분포는 광원의 스펙트럼, SOI sample 내부 계면에서의 다중반사, 광흡수 계수의 온도, 주파수 의존성 등을 고려하여 구하였으며, 열 방정식의 경계조건이 되는 wafer의 전면과 후면의 온도는 흑체복사 조건으로부터 구하였다. 내부계면에서는 전도열속(conduction heat flux)과 복사열속(radiation heat flux)에 의한 연속조건을 만족하도록 하였다.

본 문제에서의 온도분포와 열원의 분포는 상호간에 큰 영향을 주게 되므로, 두가지 변수가 일치되는 값을 보일 때까지 iteration을 계속하였다. Pyrometer을 이용하여 측정한 wafer 전면의 온도는 약1200°K이었고 이때의 simulation 결과는 1120°K 정도로 나타났다.

Abstract

A one-dimensional distribution of the temperature and the heat source in the SOI (silicon-on-insulator) multi-layer structure illuminated by tungsten lamps from both sides was obtained by solving the heat equation in steady state on a finite difference grid using successive over-relaxation method. The heat source distribution was obtained by considering such features as spectral components of the light source, multiple reflection at the internal interfaces, temperature and frequency dependence of the light absorption coefficient, etc. The front and back surface temperatures, which are boundary conditions for the heat equation, were derived from a requirement that they satisfy the radiation conditions. The radiation flux as well as the conduction flux was considered in modelling the thermal behaviour at the internal interfaces. Since the temperature and the heat source profiles are strongly dependent upon each other, the calculation of each profile was iterated using the updated profile of the other until they are consistent with each other. The experimental temperature at the front surface of the wafer as measured by pyrometer was about 1200°K, while the simulated temperature was 1120°K.

I. Introduction

Recently, much attention has been focused on the preparation of device-quality single

*正會員, 韓國科學技術院 電氣 및 電子工學科
(Dept. of Elec. Eng., KAIST)

接受日字 : 1984年 5月 19日

crystalline silicon film on insulating substrates for applications in VLSI and VHSIC devices. Compared to the laser beam, the recently proposed cw incoherent light source[1,2] has made it possible to grow single crystalline films with larger grain structure and lower point defect density at a higher throughput rate. In both cases, a knowledge of the temperature profile in the polisilicon film as well as in the silicon substrate is essential in estimating the optimal light source intensity, the thickness of various dielectric films in the wafer, and to study the physics involved in melting and recrystallization.

Temperature profile in the bulk semiconductor due to the laser beam was obtained analytically by several workers.[3,4,5] When the light source is not monochromatic and the temperature dependence of the light absorption coefficient has to be considered, the solution can only be obtained using an iterative numerical method. Lietola et al.[1] calculated the temperature profile in the bulk silicon in the 'heat sink' mode, where the backside of the silicon wafer is at a certain fixed temperature.

An experimental scheme for recrystallizing polysilicon film is shown in Fig. 1. A 0.5μm thick polysilicon film was deposited on the 0.5 μm thick SiO_2 layer which was thermally grown in the silicon wafer. A dielectric capping film, which is 2 μm thick CVD SiO_2 in Fig. 1, is usually deposited on top of the polysilicon film to prevent the impurity contamination and to act as a mechanical support. The wafer sits on a glass support within a glass chamber being continuously flushed with argon gas. The wafer is heated from the backside up to 900°C-1100°C due to the illumination from the bottom tungsten lamp. A molten zone is created in the polysilicon film by the top tungsten lamp focused on the front surface, and scanned at the velocity of 0.1~1mm/sec. The width of the focused beam perpendicular to the scanning direction is about 2.5 cm, and the length in the scanning direction is about 4mm.

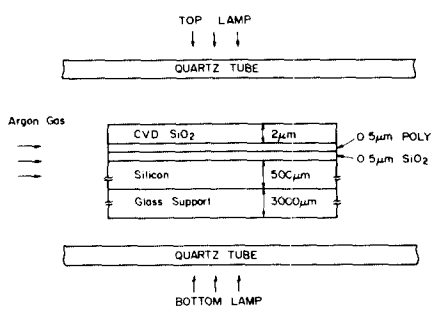

Fig. 1. Schematic view of experimental setup for recrystallization of polysilicon film.

II. Heat Source Profile

The spectral power distribution of the tungsten lamp at 2800°K as derived from the black body radiation function and the spectral emissivity data of tungsten[6], is shown in Fig. 2. In this simulation, we considered only the spectral components within the range, (0.4 μm, 3.0 μm). It is assumed that the light energy absorbed in silicon is totally converted to heat source, and the absorption in SiO_2 is negligible. The absorption coefficient of silicon, α, is a function of wavelength and temperature and is given by[7,8]

$$\alpha(\lambda,T) = 6000 \cdot \left| \frac{(E-E_g(T)-0.0575)^2}{1-\exp(-670/T)} + \frac{(E-E_g(T)+0.0575)^2}{\exp(670/T)-1} \right|,$$

where $E_g(T)=1.17-\dfrac{4.73\times10^{-4}T^2}{T+636}$(eV).

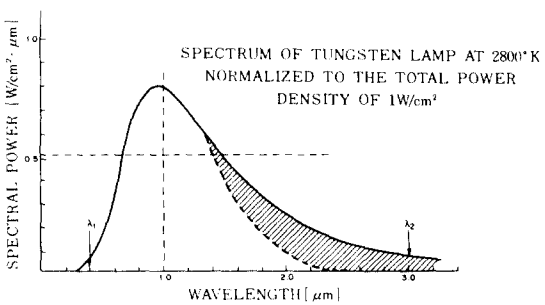

Fig. 2. Spectrum of tungsten lamp at 2800°K normalized such that total power is 1W/cm^2. The shaded region denotes the portion of the spectrum that would pass through 4 μm thick silicon film.

A simple method to calculate the heat source profile due to the top lamp (see Fig. 1) is illustrated in Fig. 3. In Fig. 3(a), the front surface of the wafer (the interface between air and the capping oxide) is placed at x=0. A very thin (≅ 300Å) Si_3N_4 film is quite commonly used along with the SiO_2 to act as capping layer, but it can be regarded as a part of SiO_2 or neglected because the refractive index of Si_3N_4 is quite close to that of SiO_2(≅2.0) and its thickness is negligible. Reflection occurs at the material interfaces: the oxide 1/poly interface ($x=L_1$), the poly/oxide 2 interface ($x=L_2$) and the oxide 2/bulk silicon interface ($x=L_3$). I_o is the intensity of light incident on the surface (x=0), and the part of I_o transmitted at x=0 is represented by I_o'. Since the incoming light, I_o', will undergo multiple internal reflections at every material interface, the signal flow graph as shown in Fig. 3(b) is introduced to obtain the light intensity as a function of location. Reflectivity at the material interfaces is a function of the refractive indices of the two neighboring materials and is not a quantity dependent on the propagating direction of the light. Reflectivities at x=0, L_1, L_2, and L_3 are represented in Fig. 3(a) as R_s, R_1, R_2 and R_3, respectively. The actual values used in the simulation are shown in Table 1, which were obtained from references [9, 10]. These values are all assumed to be constant throughout the wavelength range (0.4 μm, 3.0 μm) considered here.

Table 1. Reflectivity values at various interfaces.

Solid Si/SiO_2 interface	0.15
Solid Si/air interface	0.3
Liquid Si/SiO_2 interface	0.6
Liquid Si/air interface	0.73
SiO_2/air interface	0.04

In Fig. 3(b), each interface has two points associated with itself. The left point denotes the intensity of light traveling to the left, and the right one denotes the intensity of light traveling to the right. For example, I_{1r} is the intensity of light at $x=L_1$, traveling to the left, and I_{1p} is th intensity of light at $x=L_1$, traveling to the right. The term I_{1r} can be considered the sum of the reflected component, R_1I_o' while the term I_{1p} represents the sum of $AR_1 \cdot I_{2r}$ and $(1-R_1)I_o'$, where A denotes the attenuation in the polysilicon film given by

$$A=\exp\left|-\int_{L_1}^{L_2}\alpha(x)\,dx\right|$$

The light intensity in the polysilicon film, $I_a(x)$, can be written as

$$I_a(x)=I_{1f}\cdot\exp\left|-\int_{L_1}^{x}\alpha(x')dx'\right|+ I_{2r}\cdot\exp\left|-\int_{x}^{L_2}\alpha(x')dx'\right|,\quad L_1\leqslant x\leqslant L_2, \quad \text{eq.(1)}$$

and the light intensity in the bulk silicon, $I_b(x)$, can be written as

$$I_b(X)=I_{3f}\cdot\exp\left|-\int_{L_3}^{x}\alpha(x')dx'\right|,\ x\geqslant L_3 \quad \text{eq. (2)}$$

I_{1f}, I_{2r} and I_{2f} are obtained by solving a set of equations (3) thru (6), represented by the flow graph in Fig. 3(b).

$$I_{1f}=(1-R_1)\,I_o' + AR_1\cdot I_{2r} \qquad \text{eq. (3)}$$

$$I_{2r}=AR_2\cdot I_{1f}+(1-R_2)I_{3r} \qquad \text{eq. (4)}$$

$$I_{2f}=A(1-R_2)I_1+R_2\cdot I_{3r} \qquad \text{eq. (5)}$$

$$I_{3r}=R_3\cdot I_{2f} \qquad \text{eq. (6)}$$

The resulting values for I_{1f}, I_{2r}, and I_{3f} subscript are

$$I_{1f}=\frac{1-R_1}{1-\beta}I_o' \qquad \text{eq. (7)}$$

$$I_{2r}=\frac{1-R_1}{AR_1}\cdot\frac{\beta}{1-\beta}\cdot I_o' \qquad \text{eq. (8)}$$

$$I_{3f}=\frac{A(1-R_1)}{1-\beta}\cdot\frac{(1-R_2)(1-R_3)}{(1-R_2R_3)}\cdot I_o', \quad \text{eq. (9)}$$

$$\text{where } \beta=A^2R_1\cdot\left|\frac{R_3(1-R_2)^2}{1-R_2R_3}\right|$$

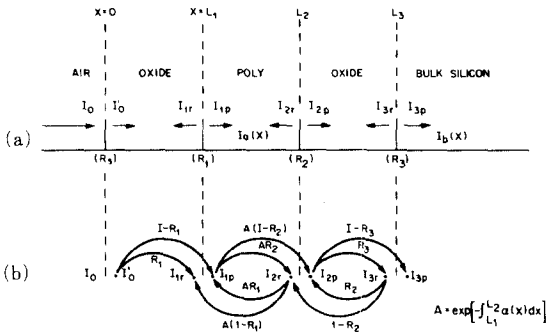

Fig. 3. (a) Light components in the frontal region of the wafer.
(b) Flow graph of the light components.

The heat source per unit volume, A(x) which has a unit of W/cm^3, is equal to the decrement of the light intensity (unit: W/cm^2) per unit length, i.e.,

$$A(x)=\frac{dI(x)}{dx} \quad \text{eq. (10)}$$

According to the definition, $dI(x)=\alpha(x)\cdot I(x)$. I(x), for the absorption coefficient, $\alpha(x)$, the heat source per unit volume, A(x), can be represented by

$$A(x)=\alpha(x)\cdot I(x) \quad \text{eq. (11)}$$

Since the absorption coefficient, α, is a strong function of wavelength and temperature (which is again a function of position, x), eq.(11) can be generalized to incorporate the wavelength dependence;

$$A(\lambda,x)=\alpha(\lambda,x)\cdot I(\lambda,x) \quad \text{eq. (12)}$$

If we assume that spectral distribution of the incoming light is $F(\lambda)$, the total heat source, A(x), generated by the incoming light is given by the integral of the spectral components within the wavelength region (λ_1, λ_2), that is,

$$A(x)=\int_{\lambda_1}^{\lambda_2} A(\lambda,x)\cdot F(\lambda)\,d\lambda \quad \text{eq. (13)}$$

The procedure for obtaining A(x) is implemented in the subroutine TSOURCE, and its flow chart is shown in Fig. 4.

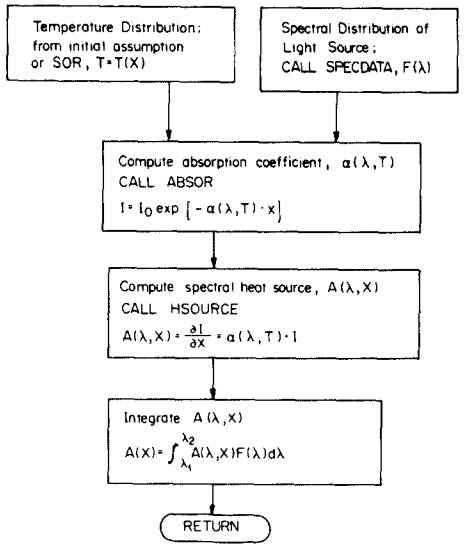

Fig. 4. Flow chart of the subroutine TSOURCE. (Calculation of the heat source profile).

III. Temperature Profile

The temperature profile is calculated by solving the heat equation.

$$-\nabla\cdot(K\nabla T)=A \quad \text{eq. (14)}$$

Where K denotes the thermal conductivity, T, the temperature, and A is the heat source term as derived in section II.

Equation (14) was solved in one dimension on a finite difference grid using the SOR (successive over relaxation) algorithm. Three different mesh spacing were used to cover the whole region as illustrated in Fig. 5(a). The frontal region, from x=1 to x=LM1, is discretized by the finest mesh ($h_1=0.05$ μm)

and the mesh size for the bulk silicon (h_2) is 3.125 μm., and that for the supporting glass is 50 μm. The mesh size discontinuity points are chosen such that they do not coincide with any material interfaces.

It is assumed that the thermal conductivity of solid silicon is 0.23 W/cm °K, and that of liquid silicon (above the melting point of silicon 1689 °K) is 0.67 W/cm °K. The three-point finite difference scheme to solve the heat equation at the i-th point is illustrated in Fig. 5(b) and the equation to be solved is

$$K_i\left|\frac{T_i-T_{i+1}}{h_2}-\frac{T_{i-1}-T_i}{h_1}\right|=\frac{h_1+h_2}{2}A_i \quad \text{eq. (15)}$$

We incorporated the SOR algorithm to solve the equation (15);

$$T_i^{(n+1)}=(1-\omega)\,T_i^{(n)}+\omega\left|\alpha_1 T_{i+1}^{(n)}+\alpha_2 T_{i-1}^{(n+1)}+\frac{h_1 h_2}{2K_i}A_i\right| \quad \text{eq. (16)}$$

Where $\alpha_1=\frac{h_1}{h_1+h_2}$, $\alpha_2=\frac{h_2}{h_1+h_2}$, and ω is the over-relaxation factor ($1\leqslant\omega<2$). The super-script in eq.(16) denotes the number of iterations.

When the mesh size is uniform, i.e., $h_1=h_2\equiv h$, eq.(16) is simplified as

$$T_i^{(n+1)}=(1-\omega)T_i^{(n)}+\frac{\omega}{2}\cdot\left|T_{i+1}^{(n)}+T_{i-1}^{(n+1)}+\frac{h^2}{K_i}A_i\right| \quad \text{eq. (17)}$$

While the equation (16), or (17), is sufficient to describe the thermal behavior of the bulk of material, the black body radiation term has to be considered additionally at the material interfaces to account for the heat exchange due to radiation.

The net radiation flux, F_{rad}, at the material interface can be written as

$$F_{rad}=\sigma\cdot|\epsilon_1-\epsilon_2|\cdot T^4 \quad \text{eq. (18)}$$

where σ is the Stefan-Boltzman constant, 5.67×10^{-12} W·cm^{-2}·°K^{-4}, and $|\epsilon_1-\epsilon_2|$ is the absolute difference of the emissivities of two neighboring materials. Therefore, Eq.(14) has to be modified at the interfaces at Eq.(19);

$$-\nabla\cdot(K\nabla T)=A-\sigma T^4\,|\epsilon_1-\epsilon_2| \quad \text{eq. (19)}$$

Newton's method was used to solve the eq.(19) which is nonlinear in T.

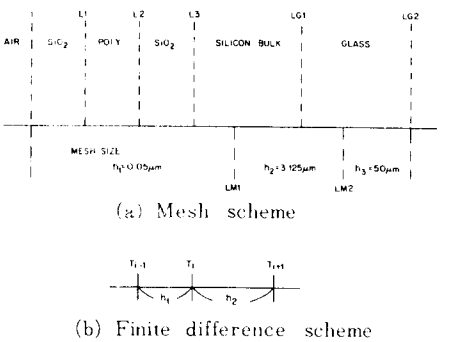

(a) Mesh scheme

(b) Finite difference scheme

Fig. 5. (a) Allocation of mesh size for each region.
(b) Finite difference scheme.

Although it is generally believed that the emissivity of silicon, ϵ_{si}, is a function of wavelength and temperature, the emissivity data available from the literature fall short of covering the region of our interest. Reference [11] covers the data from T=1000°K to 1688°K for one wavelength λ = 0.65 μm. Another set of data is available from [12] for the range 0.3 μm $\leqslant\lambda\leqslant$15$\mu$m, but only for temperatures below 1073°K. Assuming ϵ_{si} is a slowly varying function of both wavelength and temperature, we extrapolated the avilable data to obtain a constant value of ϵ_{si}=0.5 in the region of interest. On the other hand, total emissivity of SiO_2 was assumed to be 0.18 while that of air was assumed to be 0.1.

In the following we consider the front surface (the interface between air and the capping SiO_2 film) and the back surface (the interface between glass support and air). If

the temperature values and/or their derivatives are known at both boundaries, the equation can be solved unambiguously for the whole region. In our case, the boundary conditions at the front and the back surfaces are specified by the conduction flux and the radiation flux. As an example, the flux continuity at the front surface can be written as

$$F_{con} = F_{rad} \qquad \text{eq. (20)}$$

$$\text{where } F_{con} = K \cdot \frac{T_2 - T_1}{h} \qquad \text{eq. (21)}$$

$$\text{and } F_{rad} = \sigma \epsilon T_1^4 \qquad \text{eq. (22)}$$

T_1 denotes the the surface tempersture, and T_2, the temperature at the grid point just inside the surface.

Subroutine SOR calculates the temperature profile given the heat source profile data and the front surface temperature as input data. The flow chart of SOR is shown in Fig. 6. The heat source profile comes from subroutine TSOURCE as explained in section II. The front surface temperature T_1, is an input parameter to SOR which is initially set to an arbitrary value and subsequently improved by iteration. The accuracy of T_1 can be measured by a relative error, δ,

$$\delta = \left| \frac{F_{con} - F_{rad}}{F_{con}} \right| \qquad \text{eq. (23)}$$

The ℓ-th guess for T_1, T_1^{ℓ} is calculated using two previous guesses for T_1 and the associated errors;

$$T_1^{\ell} = \frac{\delta^{\ell-2} \cdot T_1^{\ell-1} - \delta^{\ell-1} \cdot T_1^{\ell-2}}{\delta^{\ell-2} - \delta^{\ell-1}} \qquad \text{eq. (24)}$$

Equation (24) is used to improve T_1, until the relevant error becomes sufficiently small. The use of this scheme leads to the unique convergence of the front surface temperature, regardless of the first two guesses. (Since eq. (24) improves T_1-value using two previous guesses, the first two initial guesses are made arbitrarily.)

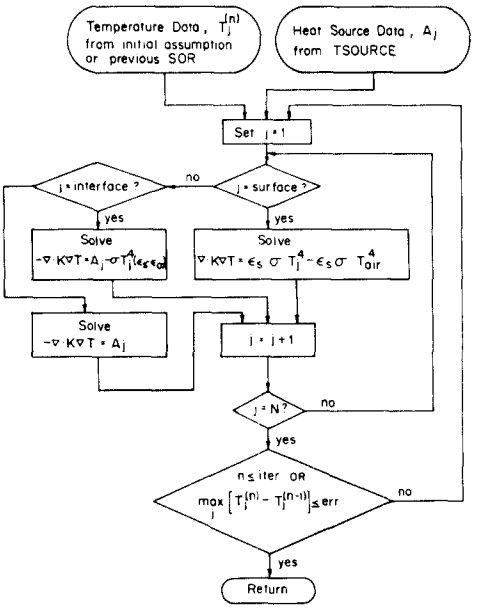

Fig. 6 Flow chart of the subroutine SOR. (Calculation of the temperature profile)

Figure 7 shows two different examples of the convergence of the temperature at the front surface of the wafer, T_1. In case I, the first two guesses are 3000°K and 1000°K, where as in case II, they are 1500°K and 2000°K, respectivey. In either case, T_1 converges to the same value, which is 1742°K. Convergence was accelerated in case II, where the initial guess of T_1 was much closer to the exact value. The decrease of the error (see

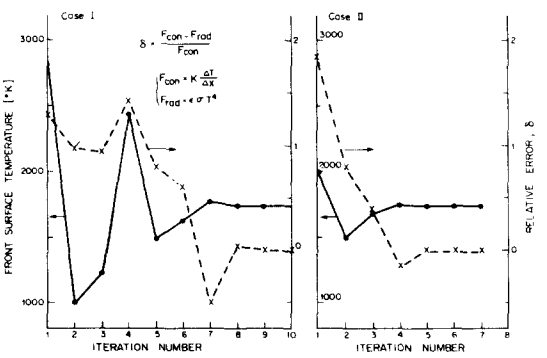

Fig. 7. Converge of the front surface temperature with iteration.

eq, (23)) was fairly monotonic in case II, while in case I the convergence was not obtained until after the seventh iteration.

Finally, the flow chart of the overall scheme is shown in Fig. 8. The outermost interation when the temperature profile. is consistent with the heat source profile.

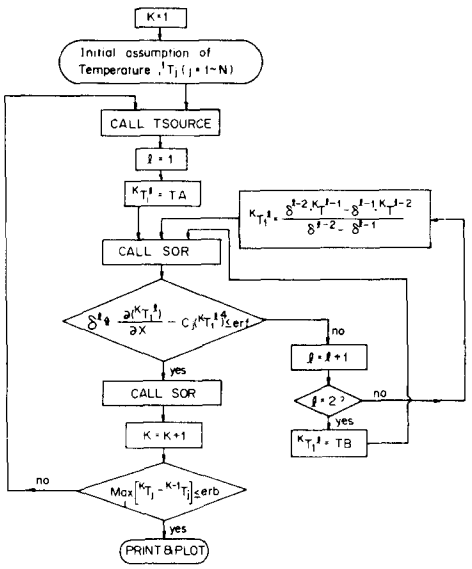

Fig. 8. Flow chart of the overall calculation Scheme.

Result

Simulation results were summarized in Fig. 9 through Fig. 11. Average CPU run time of the program written in FORTRAN IV was about 15 seconds on CRAY-1. Fig. 9 shows the calculated heat source profile as generated by absorbing the incoming light from both front-side and back-side. The solid line represents the heat source profile within the silicon wafer when the power density of the incoming light on front of the wafer, P_f (due to the top lamp in Fig. 1) is 160 W/cm^2 and the incoming power density at the backside of the wafer, P_b (due to the bottom lamp in Fig. 1) is 25.7 W/cm^2.

It is noted that most of the heat source generated within the silicon due to the top lamp is confined within the 0.5 μm thick polysilicon film, which is due to the high reflectivity (= 0.73) at the SiO_2/liquid silicon interface. Quantitatively, a total of 74.5% of the incoming power from the top lamp is reflected back into the air, 17.6% is absorbed in the 0.5 μm poly film, and the remaining 7.9% is absorbed in the bulk silicon.

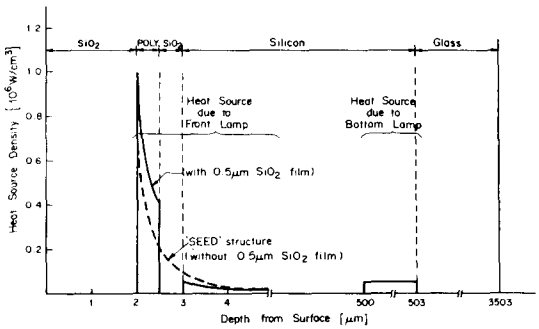

Fig. 9. Heat source profile and overall temperature profile in the original and 'seed' structure when the top lamp power is 160 W/cm^2, and the bottom lamp power is 25.7 W/cm^2.

On the other hand, 34% of the bottom lamp power is absorbed within the bulk silicon. In Fig. 1 we have shown the portion of the spectrum of tungsten lamp which will not be absorbed with 4 μm thick silicon as a shaded region. Since more than 80% of the total power is absorbed within the first 4 microns, the heat source generated by the bottom lamp can be considered to be located at the bulk silicon/glass interface. It was observed that the distribution of the heat source at the wafer backside has a negligible effect on the temperature profile in the frontal region of the wafer where our main interest lies, as long as the total magnitude of the backside heat source is conserved.

Fig. 10 shows the calculated temperature profile from the front surface of the wafer down to the backside of 3.5mm thick support glass. Three examples, denoted by (a), (b) and (c), are shown where, P_f=160 W/cm^2

and P_b=25.7 W/cm^2 in (a), while the bottom lamp was removed (P_b=0) in (b), and the top lamp was removed (P_f=0) in (c), respectively. The temperature fluctuation within the silicon wafer was less than 2°C for all examples, which seems to be due to the relatively high thermal conductivity of solid silicon (≅ 0.23 W/cm·°K) and the molten silicon (0.67 W/cm·°K) compared to the thermal conductivity of SiO_2 of 0.02 W/cm·°K.

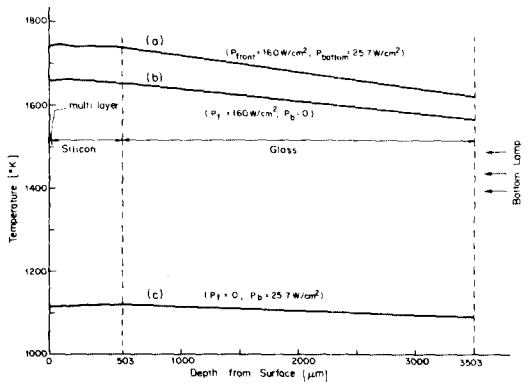

Fig. 10. Temperature profile in the original structure: (s) when P_f=160 W/cm^2 and P_b=25.7 W/cm^2, (b) when P_b=0, and (c) when P_f=0, respectively.

The temperature at the front surface of the wafer is shown to be higher than the melting point of silicon (1689 °K) for the case, (a), while (b) and (c) shows the front surface temperature below the melting point. This was also experimentally verified by observing the strip-shaped shiny molten zone on the silicon surface only for the case of (a). The actual temperature of the front surface of the wafer for the case of (c), where the top lamp was turned off, was measured using the binocular-type pyrometer to be in the range between 1150°K and 1290°K which is about 100°K higher than the simulation result (see Fig. 11). Since the optical pyrometer used in the temperature measurement cannot accurately measure the target temperature when the light from the external source is reflected at the target surface and enters the pyrometer disturbing the black-body radiation from the target, the front surface temperature was not experimentally obtained for the case of (a) and (b). Fig. 11 shows the calculated temperature at the surface of the wafer for various P_f and P_b, which can be used as a guideline for setting the power of the front lamp and the bottom lamp.

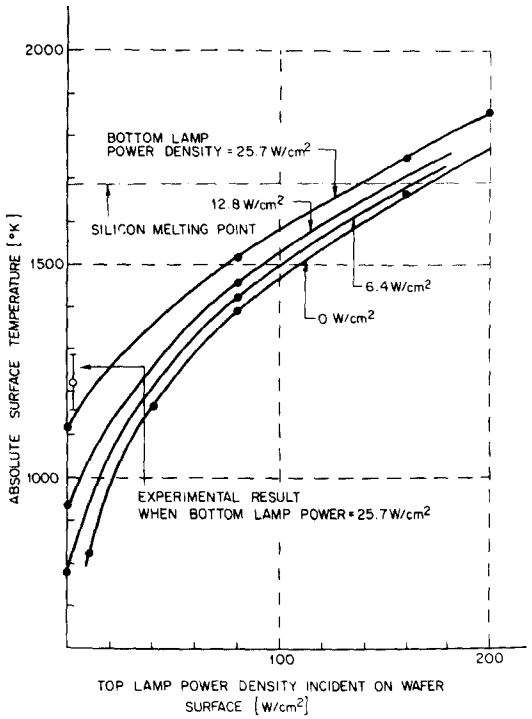

Fig. 11. Front surface temperature as a function of the top and the bottom lamp power.

A similar calculation was carried out for another silicon wafer sample which is identical to that shown in Fig. 1 except that the underlying SiO_2 film does not exist. This structure represents the 'seed' region in the recrystallization experiment where the polysilicon film is in direct contact with the bulk silicon. The calculated heat source profile in the silicon was shown as a dotted line in Fig. 9. About 12.4% of the incoming power from the top lamp was absorbed in the 0.5 μm thick polysilicon film, and 23.6% was absorbed in

the bulk silicon, while the remaining 64% was reflected back into air.

Compared to the former case when there is a SiO_2 film between polysilicon and the bulk silicon, the power absorbed in the polysilicon decreased, while that in the bulk silicon increased. This is due to the fact that there is no reflection at the polysilicon/bulk interface and the heat source is less confined in the polysilicon in the 'seed' structure.

The total percentage of the incoming power absorbed in the wafer is 36% in the 'seed' structure, and 25.7% in the former structure, and the calculated temperature at the front surface of the wafer in the 'seed' structure is about 100°C higher than that in the original structure.

An experimental observation that the width of the molten zone on the silicon wafer in perpendicular to the scanning direction broadens somewhat as the molten zone leaves the seed region and enters the original film structure seems to disagree with the above simulation result. It is to be noted that the adjustment of the relevant model parameters used in this simulation such as spectral emissivity, reflectivity, etc., which are not well documented for our interested region, could result a significant change in the calculated temperature profile, but was not tried in this work.

Conclusion

A one-dimensional program was developed to calculate the heat source and the temperature profile in a SOI multilayer structure illuminated by incoherent light. The calculation of heat source profile takes into account the multiple reflections at the internal interfaces, the spectrum of light source, and the temperature and wavelength dependence of the absorption coefficient. The inter-dependence property of the heat source and temperature upon each other is handled by continuing the solution for one with an assumption of the other until they are consistent with each other. The only input to this program is the power density of the incoming light source.

Considering the limitation coming from the measurement of the temperature, and the fact that the relevant model parameters such as spectral emissivity and reflectivity are not well characterized, it is suggested that the simulation result should be used as a guideline in the setup of experiment to predict the effect of the experimental parameters such as lamp power, film thickness, etc. on the temperature profile, rather than a means for obtaining the exact absolute temperature profile in the silicon.

Acknowledgement

The author would like to thank A. Kamgar for technical discussions and experimental data, G.E. Smith and S.M. Sze for many valuable suggestion, guidance and support throughout this work, C.K. Kim and W. Fichtner for critical reading and review of the manuscript.

References

[1] A. Lietola, R.B. Gold, and J.F. Gibbons, "Temperature rise induced in Si by continuous xenon arc lamp radiation," *J. Appl. Phys.*, vol. 53, no. 2, 1982.

[2] B.Y. Tsaur, J.C.C. Fan, M.W. Geis, D.J. Silversmith, and R.W. Moutain, "Improved techniques for growth of large-area single-crystal Si sheets over SiO_2 using lateral epitaxy by seeded solidification," *Appl. Phys. Lett.* vol. 39, no. 7, pp.561-563, 1981.,

[3] M. Lax, "Temperature rise induced by laser beam," *J. Appl. Phys.*, vol. 48, no. 9, pp.3919-3924, 1977.

[4] M. Lax, "Temperature rise induced by a laser beam, the nonlinear case," *Appl. Phys. Lett.*, vol. 33, no.. 8, pp.786-788, 1978.

[5] Y.I. Nissim, A. Lietola, R.B. Gold, and J.F. Gibbons, "Temperature distributions produced in semiconductors by a scanning ellipitcal or circular cw laser

beam," *J. Appl. Phys.*, vol. 51, no. 1, 279, 1980.

[6] See 6-199, 6-212, *American Institute of Physics Handbook.* Edited by D.E. Gray, McGraw-Hill, 1972.

[7] R.A. Smith, *Semiconductors.* Cambridge Univ., Cambridge, 2nd ed., pp.321, 1978.

[8] S.M. Sze, *Physics of Semiconductor Devices.* Wiley Interscience, 2nd ed., pp.15., 1981.

[9] M.O. Lampert, J.M. Koebel, and P. Siffert, "Temperature dependence of the reflectance of solid and liquid silicon," *J. Appl. Phys.*, vol. 52, no. 8, 1981.

[10] K.M. Shvarev, B.A. Baum, and P. W. Gel'd, "Optical properties of liquid silicon," *Sov. Phys. Solid State*, vol. 116, no. 11, May, 1975.

[11] F.G. Allen, "Emissivity at 0.65 micron of silicon and germanium at high temperatures, *J. Appl. Phys.*, vol. 28, no. 1510-2, 1957.

[12] T. Sato, "Spectral Emissivity of Silicon," *Japanese J. Appl. Phys.* vol. 6, no. 3, 1967.